

#### **OPEN ACCESS**

EDITED BY Nino Russo, University of Calabria, Italy

REVIEWED BY
Chirag Patel,
National Cancer Institute at Frederick (NIH),
United States
Daria De Raffele,
Erasmus Medical Center, Netherlands

\*CORRESPONDENCE Narasaiah Kolliputi ⊠ nkollipu@usf.edu

RECEIVED 20 September 2025 REVISED 01 November 2025 ACCEPTED 06 November 2025 PUBLISHED 19 November 2025

#### CITATION

Yata VK, Das OP, Dansana J, Gadtya A, Meher BR, Bukke SPN and Kolliputi N (2025) Designing novel peptides with amyloid- $\beta$  binding and clearance potential using BiLSTM and molecular dynamics. Front. Artif. Intell. 8:1709505. doi: 10.3389/frai.2025.1709505

#### COPYRIGHT

© 2025 Yata, Das, Dansana, Gadtya, Meher, Bukke and Kolliputi. This is an open-access article distributed under the terms of the Creative Commons Attribution License (CC BY). The use, distribution or reproduction in other forums is permitted, provided the original author(s) and the copyright owner(s) are credited and that the original publication in this journal is cited, in accordance with accepted academic practice. No use, distribution or reproduction is permitted which does not comply with these terms.

# Designing novel peptides with amyloid- $\beta$ binding and clearance potential using BiLSTM and molecular dynamics

Vinod Kumar Yata<sup>1</sup>, Om Pritam Das<sup>2</sup>, Jarmani Dansana<sup>3</sup>, Abhishikta Gadtya<sup>3</sup>, Biswa Ranjan Meher<sup>3</sup>, Sarad Pawar Naik Bukke<sup>4</sup> and Narasaiah Kolliputi<sup>5</sup>\*

<sup>1</sup>Department of Biotechnology, School of Allied and Healthcare Sciences, Malla Reddy University, Hyderabad, Telangana, India, <sup>2</sup>Department of Molecular Biology, Central University of Andhra Pradesh, Ananthapuramu, Andhra Pradesh, India, <sup>3</sup>Computational Biology and Bioinformatics Laboratory, PG Department of Botany, Berhampur University, Berhampur, Odisha, India, <sup>4</sup>Department of Pharmaceutics and Pharmaceutical Technology, Kampala International University, Western Campus, Ishaka, Uganda, <sup>5</sup>Division of Allergy and Immunology, Department of Internal Medicine, USF Morsani College of Medicine, Tampa, FL, United States

Generative artificial intelligence is transforming de novo biomolecular design, yet developing models that reliably generate functional, target-specific peptides remains a significant challenge. Here, we introduce and validate a novel two-stage Bidirectional Long Short-Term Memory (BiLSTM) framework for the generative design of short, functional peptides. Our AI pipeline is trained on full-length proteins annotated with specific Gene Ontology (GO) terms related to amyloid- $\beta$  (A $\beta$ ) interaction and is finetuned on experimentally validated peptide fragments to capture local functional motifs within a global protein context. As a proof-of-concept, we applied this framework to generate peptides targeting Aβ42, a key pathological agent in Alzheimer's disease. From 1,000 Al-generated sequences, 25 candidates were shortlisted using biophysical filters (GRAVY, instability index, Shannon entropy), and 11 were prioritized via sequence similarity analysis, designated as AI-Designed Novel Peptides (ADNP1-ADNP11). Structural modeling (AlphaFold2) and docking (pyDockWEB) against Aβ42 identified ADNP7 as the top candidate, exhibiting a highly favorable docking score (-63.33 kcal/mol), with interactions localized to Aβ's aggregation-prone regions. All-atom molecular dynamics simulations (20 ns) confirmed complex stability, and MM/PBSA analysis yielded a strong binding free energy (-50.6 kcal/mol), driven primarily by hydrophobic and aromatic interactions involving PHE12 and TRP50 in ADNP7. This work demonstrates that our fine-tuned BiLSTM architecture can successfully generate novel, stable peptide sequences with high predicted binding affinity for a therapeutically relevant target. While the training data included proteins associated with Aβ clearance (GO:0097242), only binding interactions were computationally validated; clearance potential remains a hypothesis for future experimental testing. This study establishes a generalizable, Aldriven pipeline for functional peptide design, with broad applicability across therapeutic discovery and synthetic biology.

#### KEYWORDS

deep learning, BiLSTM, peptide design, amyloid- $\beta$ , gene ontology annotation, molecular dynamics

## 1 Introduction

Alzheimer's disease (AD) is a progressive neurodegenerative disorder associated with the accumulation of amyloid- $\beta$  (A $\beta$ ) aggregates (Finder and Glockshuber, 2007; Scheltens et al., 2021). Among its isoforms, Aβ42 is particularly prone to aggregation and neurotoxicity, driving synaptic dysfunction, oxidative stress, and neuroinflammation that contribute to cognitive decline (Younkin, 1998; Mayeux et al., 2003; Kuperstein et al., 2010). Despite extensive efforts with small molecules, monoclonal antibodies, and enzymebased clearance strategies, clinical outcomes remain limited due to poor blood-brain barrier (BBB) penetration and insufficient targeting of oligomeric or fibrillar Aβ species (Levites et al., 2006; Weggen et al., 2007; Miners et al., 2008; Citron, 2010; Nie et al., 2011). Peptide-based therapeutics have emerged as promising alternatives, offering tunable specificity, reduced immunogenicity, and comparatively favorable BBB permeability relative to larger biologics (Funke and Willbold, 2012; Goyal et al., 2017). Their modularity allows for rational design and fine-tuning of affinity and selectivity (McGregor, 2008; Kaspar and Reichert, 2013). However, the development of multifunctional peptides that combine strong Aβ binding with stability and clearance potential remains challenging, largely due to the conformational heterogeneity of Aβ assemblies (Tomaselli et al., 2006; Fändrich et al., 2009). Previous efforts have explored peptidomimetics, binderblocker sequences targeting motifs such as KLVFF, and mimetic immunotherapies, but these approaches often rely on predefined motifs or rational engineering, limiting the discovery of truly novel candidates (Lowe et al., 2001; Chafekar et al., 2007; Morgan, 2011; Goyal et al., 2017; França et al., 2024).

Recent advances in artificial intelligence (AI) provide new opportunities to address these challenges by incorporating large biological datasets and machine learning/ deep learning algorithms (Fabrizio et al., 2021). LSTM-based models have been applied to identify bioactive motifs, CNN-BiLSTM hybrids to predict multifunctional peptide activities, and generative frameworks to design antiviral peptides (Fabrizio et al., 2021; Xiao et al., 2021; Li et al., 2022). Docking and molecular dynamics (MD) simulations have further elucidated Aβ interaction mechanisms (Urbanc et al., 2004; Mandal et al., 2006; Zhang et al., 2021). Yet, most approaches remain fragmented, focusing either on predictive modeling or structural analysis without fully integrating AI-driven peptide generation with physics-based validation.

To overcome these limitations, we developed a two-stage Bidirectional LSTM (BiLSTM) framework trained on proteins annotated for A $\beta$  binding and clearance (GO:0001540 for A $\beta$  binding and GO:0097242 for A $\beta$  clearance), followed by finetuning with short peptide fragments to capture therapeutically

Abbreviations: AD, Alzheimer's Disease;  $A\beta$ , Amyloid-beta;  $A\beta42$ , Amyloid-beta 42; ADNP, Amyloid-Degrading Novel Peptide; BiLSTM, Bidirectional Long Short-Term Memory; BBB, Blood-Brain Barrier; CNS, Central Nervous System; GO, Gene Ontology; GRAVY, Grand Average of Hydropathicity; hIAPP, Human Islet Amyloid Polypeptide; MD, Molecular Dynamics; MM/PBSA, Molecular Mechanics Poisson-Boltzmann Surface Area; PDB, Protein Data Bank; PME, Particle Mesh Ewald; Rg, Radius of Gyration; RMSD, Root Mean Square Deviation; RMSF, Root Mean Square Fluctuation: VMD, Visual Molecular Dynamics.

relevant motifs. From 1,000 generated sequences, we applied multi-level filtering incorporating physicochemical properties, sequence diversity, structural prediction, docking, and MD simulations. Eleven candidates (ADNP1-ADNP11) were identified, with ADNP7 showing the most favorable stability and binding profile against A $\beta$ 42. Collectively, this study introduces an AI-guided pipeline that integrates generative deep learning with structural and energetic validation, offering prioritized peptide leads for AD and a broadly applicable strategy for therapeutic peptide discovery.

# 2 Methods

# 2.1 Study design and architecture

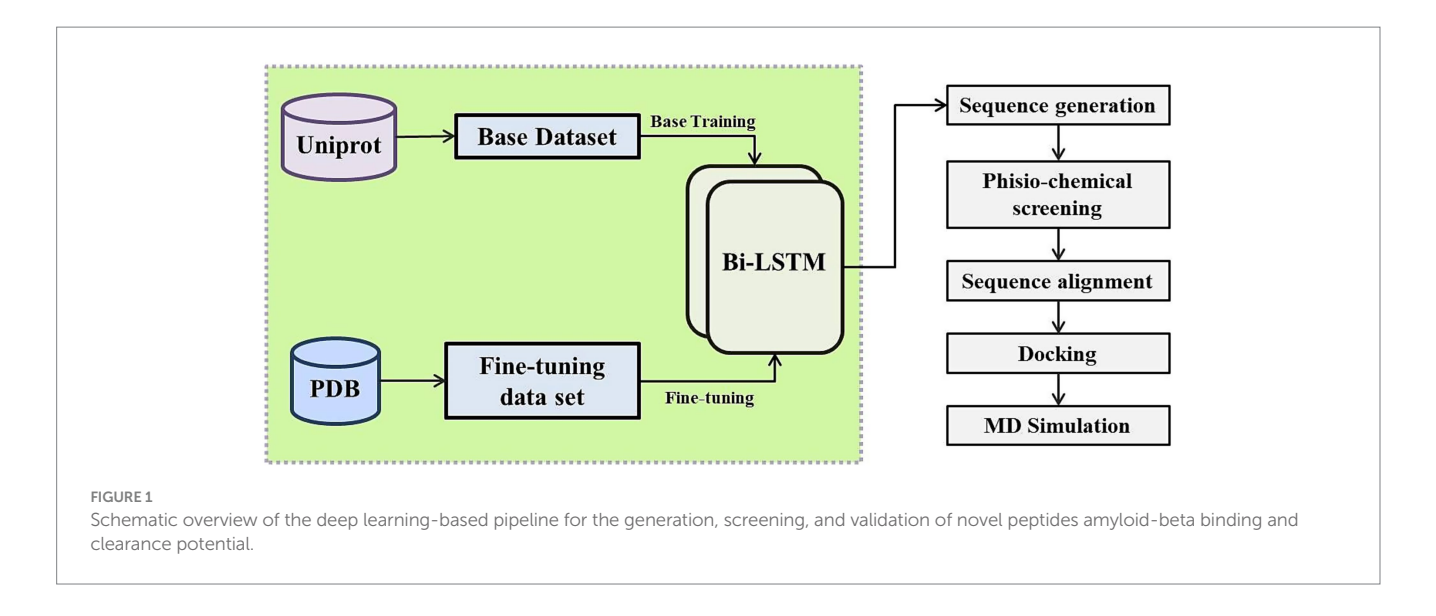
This study introduces a novel, end-to-end computational framework for the AI-driven generative design of functional peptides, demonstrated through the targeted generation of peptides predicted to bind amyloid- $\beta$  (A $\beta$ 42). The architecture is centered on a two-stage Bidirectional Long Short-Term Memory (BiLSTM) (Berglund et al., 2015) generative model, explicitly designed to bridge the gap between high-level biological function (encoded via Gene Ontology annotations) and local, therapeutically relevant peptide motifs. The pipeline is modular, reproducible, and generalizable; while applied here to AB, it can be readily adapted to other protein targets by substituting the training dataset and validation structure. At its core, the BiLSTM generative model (Berglund et al., 2015) learns to predict peptide sequences by modeling the conditional probability distribution of amino acid residues in a sequence. Formally, the probability of generating a peptide sequence  $a = (a_1, a_2, ..., a_T)$  of length, *T* is factorized as the product of conditional probabilities:

$$P(a) = \prod_{t=1}^{T} P(a_t|,...;a_1|,...;a_2|,...;...|,...;a_{t-1}|,...;\theta)$$

where,  $a_t$  represents the amino acid at position-t, and,  $\theta$  denotes the model parameters learned during training. This autoregressive modeling enables the BiLSTM to capture complex sequence dependencies in both forward and backward directions, crucial for generating biologically meaningful peptides.

The overall workflow consists of four tightly integrated phases: (1) generative modeling via the fine-tuned BiLSTM network trained initially on full-length functional proteins and subsequently refined on short peptide fragments; (2) multiparameter biophysical screening to prioritize stable, non-repetitive, and novel sequences; (3) structural modeling and rigid-body docking to assess binding potential against A $\beta$ 42; and (4) all-atom molecular dynamics simulations coupled with MM/ PBSA energetic profiling to validate complex stability and interaction mechanisms. This design ensures that AI-generated outputs are not only novel and diverse but also rigorously validated across sequence, structure, and dynamics levels prior to experimental testing (see Figure 1).

The core innovation lies in the two-stage training strategy: initial exposure to broad functional contexts (GO:0001540 for A $\beta$  binding and GO:0097242 for A $\beta$  clearance) (Ashburner et al., 2000) followed by fine-tuning on compact, experimentally



resolved peptide fragments. This approach enables the model to generate short sequences (<100 residues) that retain essential functional signatures without relying on direct templating. All generated candidates are designated as "AI-Designed Novel Peptides (ADNP)" to accurately reflect their AI-driven origin. The pipeline's emphasis on iterative computational validation from sequence generation to dynamic stability ensures robustness and provides a template for AI-driven peptide discovery across various therapeutic domains.

# 2.2 Data obtaining and preparation

The dataset for model development was manually curated to support the generation of peptides targeting amyloid-beta pathology. It comprises experimentally validated protein and peptide sequences with known amyloid-beta binding, uptake, or degradation activity, and is organized into two distinct subsets, as summarized in Table 1: The Background (Base) Set includes 7 full-length protein sequences retrieved from the UniProt database (The UniProt Consortium, 2021). These proteins (sequence lengths ranging from 230 to 1,019 residues) were selected for their relevance in amyloid-beta clearance pathways and used to pretrain the model on general sequence patterns and motif structures. The Finetuning (Sample) Set consists of short 6 peptide chains (≤100 residues) derived from crystallographic structures in the Protein Data Bank (PDB) (Berman et al., 2000). These peptides represent spatially resolved regions directly implicated in amyloid-beta interaction and were used to finetune the model toward generating bioactive peptides with therapeutic potential.

All sequences were derived from peer-reviewed studies and cross-validated for biological relevance. No synthetic or computationally augmented sequences were introduced.

Encoding and Sequence Windowing.

Each amino acid sequence was processed using a standard integer encoding scheme over the 20 canonical amino acids:

$$A = \{A,C,D,E,F,G,H,I,K,L,M,N,P,Q,R,S,T,V,W,Y\}$$

Given sequence  $S = (s_1, s_2, ..., s_L)$ , the encoded representation is defined as:

$$\hat{S} = (f(s_1), f(s_2), ..., f(s_L)), where f: A \rightarrow \{0, 1, ..., 19\}$$

To construct training examples for the generative model, a sliding window of length 35 was applied to each encoded sequence. For each window, the first 34 residues served as the input, and the 35th residue was used as the target token. Formally, the training pair at position i is:

$$X_i = (\hat{s}_i, \hat{s}_{i+1}, \dots, \hat{s}_{i+33}), y_i = \hat{s}_{i+34}$$

This framing defines a next-token prediction task, enabling the model to learn the conditional probability of the next amino acid given its context:

$$P(x_t|,,x_1|,,x_2|,,...|,,x_{t-1})$$

All sequences were truncated or padded to ensure consistency in length where necessary, but no structural or contextual augmentation was performed. This ensured that all training data remained biologically grounded, reflective of experimentally verified interactions with amyloid-beta.

# 2.3 Model development and training

The generative model was constructed using a bidirectional Long Short-Term Memory (BiLSTM) neural network architecture, chosen for its ability to capture long-range contextual dependencies within peptide sequences (Berglund et al., 2015). Unlike unidirectional models, BiLSTMs process input in both forward and reverse directions, making them well-suited to identifying biologically relevant sequence motifs in both N-terminal and C-terminal contexts. Peptide sequences were first integerencoded using a fixed vocabulary of the 20 standard amino acids. A

TABLE 1 Summary of protein sequences used for model training and fine-tuning, including UniProt/PDB IDs, sequence lengths, and literature references.

Background (Base) Set					
Uniprot id	Protein Name	Sequence Length	Ref.		
P10909	Clusterin	449	Narayan et al. (2012) and Yeh et al. (2016)		
P11835	Integrin beta-2	771	Jeon et al. (2008) and Choucair- Jaafar et al. (2011)		
P16671	Platelet glycoprotein 4	472	Shimizu et al. (2008) and Zhao et al. (2018)		
P30204	Macrophage scavenger receptor types I and II	458	Husemann et al. (2001)		
P35559	Insulin-degrading enzyme	1,019	Llovera et al. (2008), Shimizu et al. (2008), and Vekrellis et al. (2000)		
P35951	Low-density lipoprotein receptor	862	Kim et al. (2009) and Basak et al. (2012)		
Q9NZC2	Triggering receptor expressed on myeloid cells 2	230	Yeh et al. (2016), Zhao et al. (2018), and McQuade et al. (2020)		

Finetuning (Sample) Set						
PDB ld	Protein Name	Sequence Length	Ref.			
2FYL	alpha2- macroglobulin receptor-associated protein Chain 1	81	P (2012)			
	alpha2- macroglobulin receptor-associated protein Chain 2		Basak et al. (2012)			
6V7M	Apolipoprotein E Chain 1	100	Cho et al. (2001) and Hopkins et al.			
	Apolipoprotein E Chain 2	83				
2KNX	Low-density lipoprotein receptor- related protein 1	50	Bell et al. (2009), Kanekiyo et al. (2012, 2013), and Zhao et al. (2015)			
2KNY	Prolow-density lipoprotein receptor- related protein 1	80				

sliding window of length 35 was applied to each sequence, generating overlapping subsequences in the format  $(x_1, x_2, ..., x_{34}) \rightarrow x_{35}$  where the first 34 residues served as input and the 35th residue was used as the target label. The model was thus trained to learn the conditional probability distribution over amino acids given a preceding context window:

$$P(x_t|,,x_1|,,x_2|,,...|,x_{t-1})$$

At each position *t*, the BiLSTM model produced forward and backward hidden states defined as:

$$\vec{h}_t = LSTM_f\left(x_t, \vec{h}_{t-1}\right), \hat{h}_t = LSTM_b\left(x_t, \hat{h}_{t+1}\right)$$

The final representation at position t was obtained by concatenating these directional states:

$$h_t = \begin{bmatrix} \vec{h}_t; h_t \end{bmatrix}$$

This hidden representation was passed through two fully connected dense layers with ReLU activations, followed by a final softmax layer to output the predicted probability distribution over the 20 amino acid classes:

$$\hat{y}_t = Softmax(Wh_t + b)$$

Where W and b are the learnable weights and biases of the output layer. Model training was guided by the categorical cross-entropy loss function:

$$L = -\sum_{t=1}^{T} y_t \log(\hat{y}_t)$$

The full architecture consisted of two stacked BiLSTM layers with 256 units each, followed by two dense layers. Dropout regularization ( $dropout\ rate = 0.2$ ) was applied after each LSTM layer to mitigate overfitting. The model was trained using the Adam optimizer (learning rate = 0.001) for 150 epochs in the base phase and 45 epochs in the fine-tuning phase, with batch sizes of 30 and 62, respectively.

Training was carried out in two distinct phases. During the base phase, the model was trained on long, functionally annotated protein sequences (Table 1), enabling it to learn generalizable sequence grammar related to amyloid-beta interaction. In the second phase, the model was fine-tuned using a curated dataset of shorter peptides (<100 residues), steering its output distribution toward compact, therapeutically relevant sequences. The model was optimized using the Adam optimizer with a learning rate of  $1 \times 10^{-3}$ , a batch size of 64 for generalization, and early stopping (patience = 10) based on validation loss. Although validation split was not explicitly implemented in code due to the limited sample size, instead stability and convergence of the

model were monitored by tracking training loss across epochs and performing repeat runs to assess reproducibility. This two-phase training paradigm allowed the model to first learn the global syntax and compositional structure of bioactive peptides and then specialize in generating novel, functionally coherent, and sequence-stable peptides suitable for downstream screening.

# 2.4 Peptide generation and physicochemical shortlisting

Following fine-tuning, the trained BiLSTM model was utilized to generate novel peptide sequences through an autoregressive sampling approach. Starting with randomly constructed seed sequences derived from the training dataset, the model predicted the next amino acid token iteratively. At each step t, the model used a fixed-length context window of 35 residues and predicted the most probable next amino acid  $x_{t+1}$  based on the preceding sequence  $x_{t-34:t}$ :

$$P(x_{t+1}|, x_{t-34}|, x_{t-33}|, x_{t-34}|) = softmax(f_{BiLSTM}(x_{t-34:t}))$$

Here,  $f_{BiLSTM}$  denotes the trained network and the output is sampled via greedy decoding (argmax). This process was repeated until a complete peptide of length,  $L \in [80,100]$  residues was generated. A total of 1,000 such sequences were synthesized.

To systematically reduce the sequence space, a two-stage physicochemical screening pipeline was employed. In Stage 1, the generated sequences were partitioned into five batches of 200 each. For every peptide, the following three metrics were computed:

1 Shannon entropy *H*, measuring amino acid diversity within a sequence *s* of length *n*:

$$H(s) = -\sum_{a \in A} p(a) \log_2 p(a)$$

where A is the set of standard amino acids and p(a) is the empirical frequency of residue a in the sequence (Shannon, 1948).

2 GRAVY score *G*, calculated as the mean hydropathy index over all residues:

$$G(s) = \frac{1}{n} \sum_{i=1}^{n} h(s_i)$$

where  $h(s_i)$  is the Kyte-Doolittle hydropathy value of residue  $s_i$  (Kyte and Doolittle, 1982).

3 Instability Index *I*, which estimates *in vitro* stability based on dipeptide composition. While the precise formula involves 400 pairwise weights  $\delta(s_i, s_{i+1})$ , it is conceptually represented as:

$$I(s) = \frac{10}{n} \sum_{i=1}^{n-1} \delta(s_i, s_{i+1})$$

Higher values of I indicate greater instability; sequences with I > 40 are generally considered unstable (Guruprasad et al., 1990).

Within each batch, sequences were ranked to prioritize high Shannon entropy, moderate-to-low GRAVY, and low instability index. The top 10 sequences per batch were selected, yielding 50 candidates for further evaluation.

In Stage 2, these shortlisted peptides were compared to those in the fine-tuning dataset to ensure alignment with physicochemical properties of experimentally validated  $A\beta$ -interacting peptides. For each generated sequence p and reference peptide r, the Euclidean distance in the 2D feature space of GRAVY and instability was computed as:

$$d(p,r) = \sqrt{(G_p - G_r)^2 + (I_p - I_r)^2}$$

Each batch of 10 sequences was compared to the centroid of the fine-tuning reference distribution, and the five closest sequences per batch were retained, resulting in 25 final candidate peptides. This two-stage process ensured that the selected peptides possessed sequence diversity, biophysical stability, and feature similarity to known functional peptides, while maintaining novelty.

# 2.5 Sequence similarity analysis

To assess the novelty and potential functional relevance of the shortlisted peptides, sequence similarity analysis was performed using Clustal Omega, a widely accepted tool for multiple sequence alignment (Sievers and Higgins, 2014). This step ensured that the generated sequences shared meaningful similarity with known amyloid-beta-binding and degrading peptides, while still maintaining a level of novelty indicative of de novo design. The 25 shortlisted sequences were aligned against the six fine-tuning peptide chains [derived from PDB entries Clusterin (2FYL), Heat shock protein HSP 90-beta (6V7M), Metalloprotease (2KNX), and Metalloprotease domain-containing protein 3 (2KNY) using Clustal Omega with default parameters]. The alignment output provided pairwise percentage identity scores for each generated peptide against the reference chains. These scores were analyzed to identify which sequences shared the highest similarity to functionally validated peptides, serving as a proxy for potential biological relevance.

# 2.6 3D modelling and docking analysis

To assess the structural plausibility and amyloid-beta (Aβ) binding potential of the shortlisted peptides, 3D structural modeling followed by protein–protein docking was performed. The 11 peptides selected after biophysical screening and sequence similarity analysis were named as Amyloid-Degrading Novel Peptide (ADNP1–ADNP11) and were structurally modeled using the AlphaFold server (Jumper et al., 2021). Structural visualization and verification were carried out using Jmol to ensure correct folding, absence of steric clashes, and suitability for docking (Herráez, 2006). Protein–protein docking was performed using pyDockWEB, a rigid-body docking server that incorporates electrostatics, desolvation, and van der Waals scoring (Jiménez-García et al., 2013). Each modeled peptide structure was docked against the Aβ42 monomer structure retrieved from the Protein Data Bank (PDB ID: 1IYT) (Crescenzi et al., 2002). The docking protocol evaluated

multiple energy-based scoring components, including electrostatic energy, desolvation energy, van der Waals energy, and total binding energy. ADNP peptides demonstrating more negative total docking scores were interpreted to have higher binding affinities toward  $A\beta.$  Particular emphasis was placed on peptides exhibiting favorable van der Waals and desolvation scores, as these indicate better surface complementarity and solvent compatibility, both of which are crucial for stable and specific protein–protein interactions.

# 2.7 Molecular dynamics simulation of the ADNP7-A $\beta$ 42 complex

# 2.7.1 Configuration of the system and solvation

To investigate the conformational dynamics and stability of the most promising peptide, ADNP7, in complex with amyloid-beta (Aβ42), two independent all-atom molecular dynamics (MD) simulations were performed using the AMBER 18 simulation suite (Case et al., 2018). The initial docking pose of ADNP7 complexed with Aβ42 was acquired from the highest-ranking pose achieved via rigidbody docking utilizing pyDockWEB. The protein-peptide complex was preprocessed and subsequently parameterized utilizing the ff14SB force field, which is optimal for simulating folded proteins and peptides. The solvated system was constructed utilizing the tLeap module of AmberTools. Hydrogen atoms were incorporated based on normal protonation states at physiological pH. The complex was situated within a truncated octahedral box containing TIP3P water molecules, maintaining a minimum buffer zone of 10 Å surrounding the solute in every direction. This solvation model simulates a realistic watery milieu. An adequate quantity of sodium ions (Na+) was randomly introduced to equilibrate the net charge of the system. The resultant solvated and neutralized system underwent energy minimization before dynamic simulations.

## 2.7.2 Energy optimization

Energy minimization was performed in a three-step, progressively unrestrained approach to eliminate steric conflicts, alleviate stressed geometries, and stabilize the system prior to heating and equilibration. Initially, a constrained reduction of 1,000 steps was executed with harmonic restrictions (10 kcal/mol·Å²) imposed on the backbone atoms of the complex, facilitating the adjustment of solvent molecules and counterions. The subsequent phase involved restraining only the  $C\alpha$  atoms of the protein–peptide combination with the identical force constant, while the remainder of the system underwent minimization for 1,000 steps. In the last stage, all constraints were lifted, and a comprehensive system reduction was performed for 1,000 iterations to guarantee total energy relaxation. Each minimization step incorporated a blend of steepest descent and conjugate gradient methods to attain convergence and provide seamless transitions in the potential energy surface.

# 2.7.3 Heating

Subsequent to energy minimization, the system was incrementally heated from 0 K to 300 K over 70,000 steps under constant volume circumstances (NVT ensemble). In this phase, a mild harmonic

constraint (5 kcal/mol·Å²) was imposed on all heavy atoms of the solute to avert deformation of the native structure during fast temperature elevations. Langevin dynamics facilitated temperature coupling with a collision frequency of  $2\,\mathrm{ps^{-1}}$ , ensuring steady thermalization of the solvent and gradual activation of molecular movements. The gradual heating facilitated thermal equilibration of the system in a regulated manner, preventing any sudden conformational alterations.

#### 2.7.4 Equilibration

Equilibration was conducted in six meticulously structured stages to enable the system to attain thermodynamic stability regarding pressure, density, and temperature. All equilibration phases were performed under NPT ensemble circumstances utilizing the Berendsen barostat to sustain pressure at 1 atm and the Langevin thermostat to regulate temperature at 300 K. During the initial three phases (EQ-B, EQ-C, and EQ-D), the system underwent equilibration for 1,000 steps at each stage, with progressively diminishing positional restrictions on the solute atoms. These measures guaranteed the solvent and ions were adequately relaxed without disrupting the natural structure of the protein-peptide complex. The fourth equilibration phase (EQ-E) was prolonged to 20,000 steps to facilitate adequate pressure coupling and solvent density adaption. A concluding equilibration phase (EQ-F) was executed for 80,000 steps without constraints, guaranteeing the system's full relaxation under physiological conditions. At the conclusion of equilibration, the system attained stable temperature, pressure, and density, exhibiting minimal variations, and was prepared for the simulation's production phase.

## 2.7.5 Production

Two sets of 20-nanosecond molecular dynamics simulations were conducted under NPT ensemble settings to study the long-term structural dynamics and interactions between ADNP7 and Aβ42. The simulations were conducted with the pmemd.mpi by utilizing AMBER 18 package. The temperature was regulated at 300 K via the Langevin thermostat, while the pressure was controlled at 1 atm using the Berendsen barostat for both sets of MD simulations. The integration time step was established at 1 fs, and all bonds involving hydrogen atoms were restricted via the SHAKE algorithm, facilitating a stable and efficient simulation. Non-bonded interactions were computed with a 10 Å cutoff, whilst long-range electrostatics were addressed using the Particle Mesh Ewald (PME) approach to ensure precise handling of periodic boundary conditions. System coordinates were recorded every 10 picoseconds, yielding a total of 20,000 frames for the complete 20 nanosecond simulation. This trajectory data was utilized for future structural, dynamic, and energetic analyses to assess stability and binding characteristics of the peptide.

#### 2.7.6 Trajectory analysis

Post MD simulation analysis was performed with CPPTRAJ (from AmberTools18) and Visual Molecular Dynamics (VMD) to derive significant insights from the 20 ns trajectory. Root Mean Square Deviation (RMSD) computations were conducted for the backbone atoms of the complex to evaluate structural stability over

time. Root Mean Square Fluctuation (RMSF) values were calculated for each residue to assess local flexibility and pinpoint dynamic regions, especially at the binding interface. The Radius of Gyration (Rg) was observed during the simulation to assess the compactness of the ADNP7-Aβ42 complex and identify significant conformational alterations. An investigation of hydrogen bonding was performed to assess the frequency and durability of intermolecular hydrogen bonds between the peptide and the  $A\beta42$ chain, yielding insights into critical interactions that maintain the complex. For energetic assessment, MM/PBSA (Molecular Mechanics Poisson-Boltzmann Surface Area) free energy calculations were conducted utilizing MMPBSA.py on 500 typical frames selected from the final 20 ns of the trajectory. This facilitated the calculation of the binding free energy between ADNP7 and Aβ42, which was decomposed into contributions from electrostatic, van der Waals, polar solvation, and non-polar solvation energies. These analyses jointly facilitated a comprehensive knowledge of the structural stability, dynamic flexibility, and binding affinity of the ADNP7-Aβ42 complex under simulated physiological settings.

# **3** Results

# 3.1 Model training and performance

The model architecture was based on a Bidirectional Long Short-Term Memory (BiLSTM) network, chosen for its capacity to learn both upstream and downstream sequence dependencies in protein sequences. The training was performed in two stages: a base training phase using seven long A $\beta$ -related proteins from UniProt, and a fine-tuning phase using six short peptides ( $\leq$ 100 residues) derived from PDB structures. Both stages used a window size of 35 amino acids, with 34 as input and the 35th as the prediction target, enabling the model to learn contextual residue prediction.

During the base training, the model converged steadily, as reflected in the training loss and accuracy metrics. The loss decreased consistently over epochs stabilizing around 0.2–0.3, indicating improved predictive performance. Accuracy also improved progressively reaching over 0.95, demonstrating the model's growing ability to predict the next amino acid in A $\beta$ -related sequences. Fine-tuning further refined the model's predictions on shorter peptides, as evident from the sharper convergence of loss reaching less than 0.1 and a slight improvement in accuracy reaching 9.8, suggesting effective adaptation to compact sequence features relevant for therapeutic design The training performance during the base training and fine-tuning are visualized in Figure 2.

# 3.2 Sequence generation and biophysical screening

Using the fine-tuned BiLSTM model, 1,000 novel peptide sequences, each under 100 amino acids, were generated with the aim of mimicking the properties of known amyloid-beta  $(A\beta)$  binding and degrading peptides. These sequences were subjected to a two-stage

screening process based on their physicochemical properties to identify candidates with favorable biochemical stability and diversity.

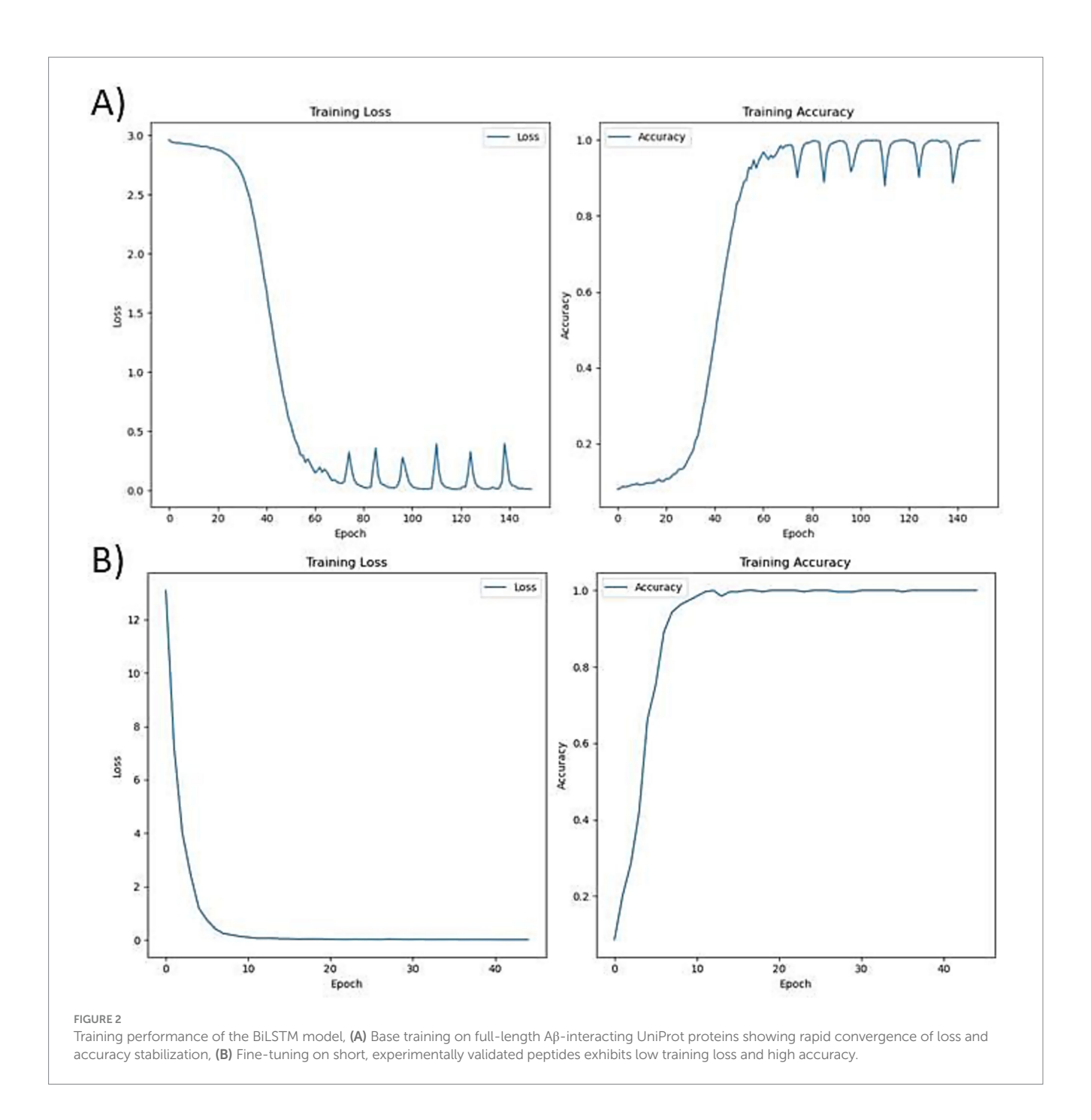
In the first screening stage, the 1,000 generated peptides were divided into five batches of 200 sequences each. Within each batch, peptides were evaluated using three key biophysical metrics: GRAVY (Grand Average of Hydropathy), instability index, and Shannon entropy. GRAVY scores were used to estimate hydrophobicity, with moderate values indicating a balance between solubility and membrane interaction. The instability index predicted peptide stability under in vitro conditions, where values below 40 are considered stable. Shannon entropy measures the diversity of amino acid usage within each sequence, favoring sequences with non-repetitive and information-rich content. Figure 3 visualizes the distributions of the biophysical metrics comparatively between the dataset sequences vs. the generated sequences. Based on a composite score integrating these three metrics, the top 10 peptides from each batch (50 total) were shortlisted. These 50 peptides were compared against the six finetuning sequences using Euclidean distance across GRAVY and instability values In the second stage biophysical screening. The goal was to retain peptides that were biophysically most similar to experimentally validated Aβ-interacting peptides. From each batch, the five closest peptides were selected, yielding a final set of 25 highconfidence candidates for downstream structural functional evaluation.

# 3.3 Sequence similarity analysis

To assess whether the 25 shortlisted peptides were novel or bore resemblance to known amyloid-beta (A $\beta$ )-interacting sequences, a comprehensive sequence similarity analysis was conducted using Clustal Omega. This analysis was intended to (i) identify evolutionary or functional resemblance to known A $\beta$ -binding and degrading sequences and (ii) confirm that the generated peptides were not trivially derived from the training data. Each of the 25 peptides was aligned with the six fine-tuning sequences used during the second training phase. The alignment scores were computed based on percent identity values returned by Clustal Omega, providing a quantitative measure of sequence-level similarity (Supplementary Table 1). Importantly, none of the peptides were exact or near-exact matches to any of the training sequences, indicating that the generative model had successfully learned abstract sequence patterns rather than memorizing specific examples (Table 2).

# 3.4 3D structure prediction and docking

To assess the structural integrity and binding potential of the top 11 peptides (ADNP1–ADNP11), we performed three-dimensional (3D) structure prediction followed by protein–protein docking. The peptide structures were predicted using the AlphaFold2 server. The predicted PDB files were extracted using Jmol for downstream analysis. For docking studies, each modeled peptide was docked against the Aβ42 peptide (PDB ID: 1IYT) using pyDockWEB. The results are summarized in Table 3, showing that all 11 peptides exhibited negative total interaction energies, indicating favorable binding. Among them, ADNP7 demonstrated

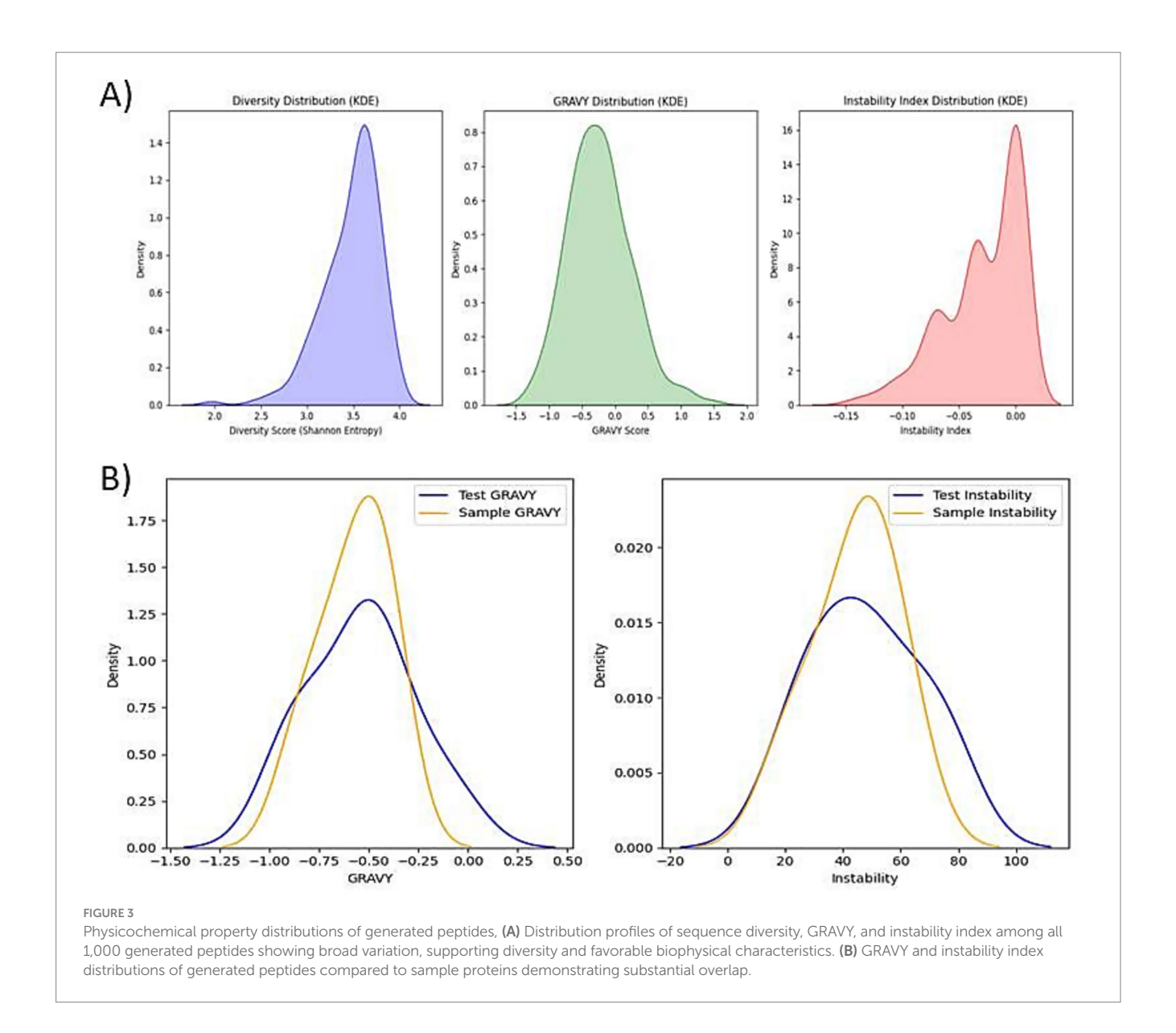


the strongest predicted interaction, with a total docking energy of -63.33 kcal/mol, outperforming both reference and other novel peptides. Other promising candidates included ADNP5 (-50.69 kcal/mol) and ADNP11 (-47.27 kcal/mol). As shown in Figure 4, ADNP7 docks within a hydrophobic cleft of A $\beta$ 42, with surface-accessible residues (including TYR69, GLY46, and LEU44) forming hydrogen bonds and hydrophobic contacts near aggregation-prone regions (e.g., residues 16–21 and 30–42) (Crescenzi et al., 2002; Tomaselli et al., 2006). The diversity in docking orientations and contact residues indicates that different peptides may engage distinct structural motifs of A $\beta$ 42, potentially interfering with its oligomerization pathways through multiple mechanisms. These findings validate the docking potential of the generated peptides and highlight ADNP7 as a particularly strong

candidate for further investigation through molecular dynamics simulations and experimental validation (Figure 4).

# 3.5 Post-MD simulation analysis

To ensure reproducibility of the MD stability assessment, two independent simulations were performed for the ADNP7–A $\beta$ 42 complex, and the structural parameters were analyzed using statistical summaries. The RMSD values remained stable across both sets (5.415 ± 1.989 Å in Set-1 and 5.555 ± 1.437 Å in Set-2), indicating consistent backbone convergence. Similar reproducibility was observed in RMSF (3.907 ± 1.673 Å vs. 2.909 ± 1.703 Å) and Rg values (34.083 ± 3.589 Å vs. 42.288 ± 5.536 Å), confirming that the overall



compactness and residue-level flexibility remained comparable between simulations. These results validate that the structural stability findings are reliable and not dependent on a single MD trajectory (Table 4).

# 3.5.1 Structural stability assessment: RMSD analysis

The Root Mean Square Deviation (RMSD) plots of the backbone  $C\alpha$  atoms for both MD replicates (Set-1 and Set-2) were examined over the 20 ns trajectory to assess the overall structural stability of the ADNP7–A $\beta$ 42 complex. Figure 5 demonstrates that both simulation sets exhibit an initial increase in RMSD values over the first 2–4 ns, signifying structural adaptation and relaxing of the complex inside the solvated environment. Set-1 demonstrated a moderate increase in RMSD, stable around 4–6 Å until around 12 ns, followed by a more significant rise exceeding 8 Å in the final nanoseconds. Set-2 exhibited a little accelerated deviation initially, with RMSD values of 6–7 Å during the 4–8 ns interval, then sustained a more uniform fluctuation pattern of 5–7 Å beyond

10 ns. Notably, Set-1 demonstrated increased structural deviation in the later phases of the simulation, whereas Set-2 displayed greater volatility in the initial stages but sustained modest stability thereafter. The disparities can be ascribed to the randomized initial velocities (ig values), which may have resulted in divergent conformational sampling pathways. Both runs ultimately converged to structurally diverse but stable conformations, highlighting the dynamic plasticity of the complex and validating the necessity for many independent simulations.

# 3.5.2 Residue flexibility: RMSF analysis

To analyze residue-level motion inside the complex, the Root Mean Square Fluctuation (RMSF) was calculated for all C $\alpha$  atoms during the trajectory (Figure 6). Both sets exhibited analogous fluctuation patterns throughout the sequence, with slight discrepancies in size. The N-terminal and C-terminal portions of the complex exhibited the greatest variations, as anticipated due to their exposed and unstructured characteristics. The interface between the ADNP7 peptide and A $\beta$ 42 (about residue locations ~85–90) had a

TABLE 2 Sequence identity and alignment scores of 11 shortlisted ADNP peptides with six reference proteins used in fine-tuning.

Sequence	Given	Sednence		Align	Alignment score with sample sequences	ple sequences		
name	sednence id	Length	2FYL_1 Chain	2FYL_2 Chain	6V7M_1 Chain	6V7M_2 Chain	2KNY_1	2KNX_1
ADNP1	Sequence_5	100	15.22	15.09	14.52	12.77	19.51	17.14
ADNP2	Sequence_48	86	15.09	28.33	17.24	22.97	35.19	20.69
ADNP3	Sequence_146	95	27.78	24.07	13.16	27.12	34.72	22.73
ADNP4	Sequence_196	91	15.79	20.45	19.64	14.89	26.09	25
ADNP5	Sequence_211	100	15.91	25	29.63	14	23.4	25
ADNP6	Sequence_220	85	13.33	19.23	10.71	12.5	15.79	11.11
ADNP7	Sequence_222	88	20	18.87	10.61	23.73	16.33	14.71
ADNP8	Sequence_277	85	22.22	25.45	9.52	23.08	21.74	29.03
ADNP9	Sequence_312	84	22.64	21.88	10.94	23.91	24.49	18.75
ADNP10	Sequence_405	98	20	17.24	20.41	24.24	31.43	32.65
ADNP11	Sequence_431	86	16.39	23.73	16.67	16.92	21.28	25

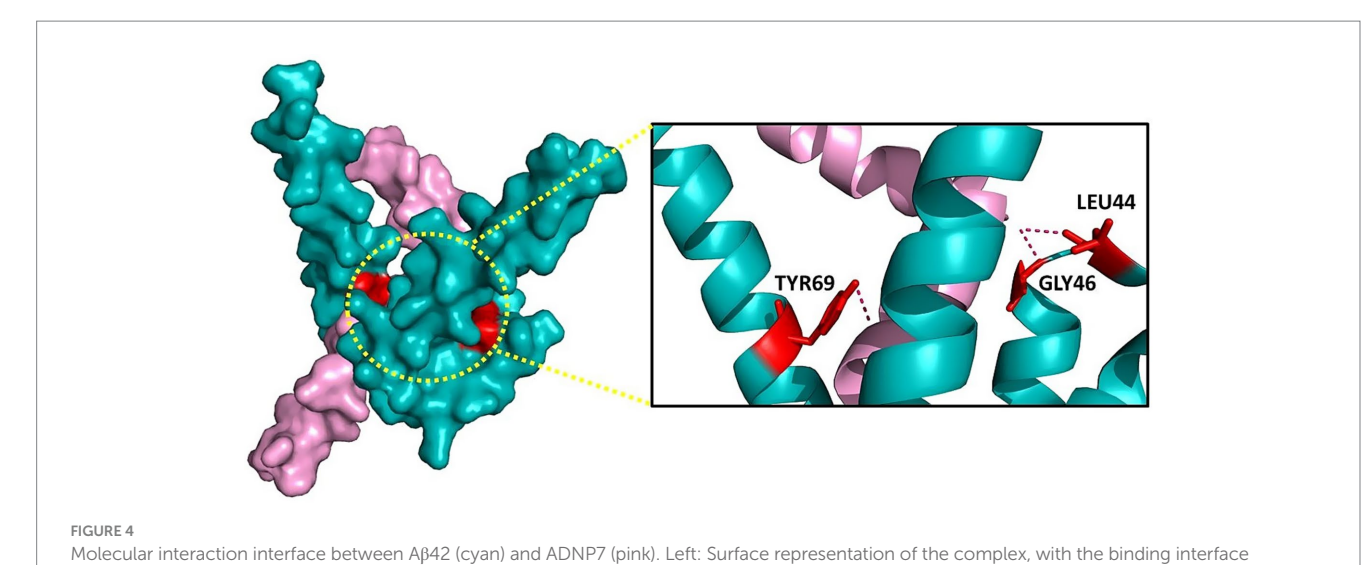
TABLE 3 Electrostatic, desolvation, van der Waals, and total docking energies for benchmark and novel peptides docked with  $A\beta42$ .

Protein name	Electrostatics	Desolvation	Van der Walls	Total			
Sample proteins docking with amyloid beta							
2FYL_1	-16.754	-23.368	25.731	-37.549			
2FYL_2	-24.065	-18.388	30.901	-39.363			
6V7M_1	-19.568	-36.483	84.015	-47.649			
6V7M_2	-28.169	-13.155	54.088	-35.915			
2KNX	-11.968	-22.406	-3.73	-34.748			
2KNY	-33.549	-5.999	73.728	-32.175			
Novel proteins docking with amyloid beta							
ADNP1	-14.744	-33.989	45.624	-44.17			
ADNP2	-8.157	-35.979	43.011	-39.835			
ADNP3	-15.734	-17.356	69.241	-26.166			
ADNP4	-6.287	-41.294	46.051	-42.976			
ADNP5	-7.547	-47.401	42.62	-50.686			
ADNP6	-18.868	-20.42	31.8	-36.109			
ADNP7	-8.601	-63.07	83.436	-63.328			
ADNP8	-18.609	-30.219	90.393	-39.789			
ADNP9	-11.687	-27.916	77.333	-31.87			
ADNP10	-3.306	-46.824	51.999	-44.93			
ADNP11	-12.172	-41.706	66.046	-47.273			

prominent peak in Set-1, suggesting localized flexibility potentially attributable to loop or linker dynamics. The RMSF values were predominantly lower in the ADNP7 segment (residues 1–88, highlighted in yellow), indicating stable anchoring and a structured conformation of the designed peptide when associated with the A $\beta$ 42 chain. Conversely, the A $\beta$ 42 segment (residues 89–130, highlighted in green) exhibited greater variations, especially in Set-1, with peaks near terminal residues and in areas associated with aggregation. Set-2 exhibited reduced fluctuations in the same locations, potentially indicating alternative hydrogen bonding or inter-residue packing resulting from the variation in velocity seeds. The data indicate that ADNP7 binding results in a partial stabilization of A $\beta$ 42; however, terminal residues and flexible loops remain mobile, potentially affecting aggregation behavior.

# 3.5.3 Compactness: Radius of Gyration (Rg) analysis

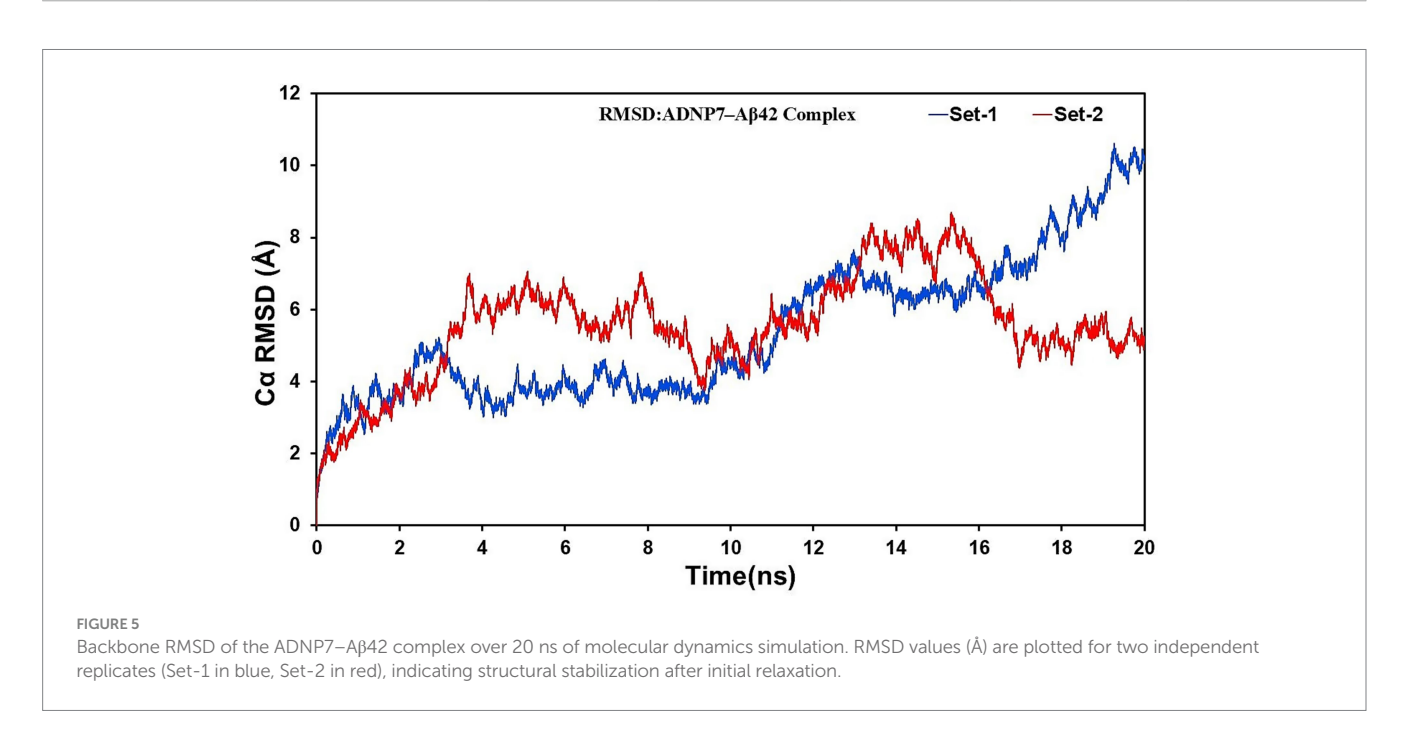
The Radius of Gyration (Rg) values were computed to assess the overall compactness and folding dynamics of the complex over time (Figure 7). Both sets exhibited stable Rg variations, varying between 30 and 50 Å. Set-1 exhibited a more compact conformation throughout the simulation, averaging approximately 35–38 Å, whereas Set-2 demonstrated marginally elevated Rg values (40–50 Å) during several intermediate intervals (notably 4–8 ns and 12–16 ns), suggesting transient expansion of the complex. The elevated Rg values noted in Set-2 may correlate with localized unfolding phenomena or enhanced solvent exposure in the flexible domains of Aβ42. Both simulations ultimately reverted to similar



highlighted by a yellow dotted circle. Right: Zoomed-in view showing key interacting residues from ADNP7- TYR69, GLY46, and LEU44, forming hydrogen bonds (dashed lines) and hydrophobic contacts with Aβ42. Residues are shown as sticks for clarity.

TABLE 4 MM/GBSA binding free energy (Kcal/mol) components of ADNP7-Aβ42 complex.

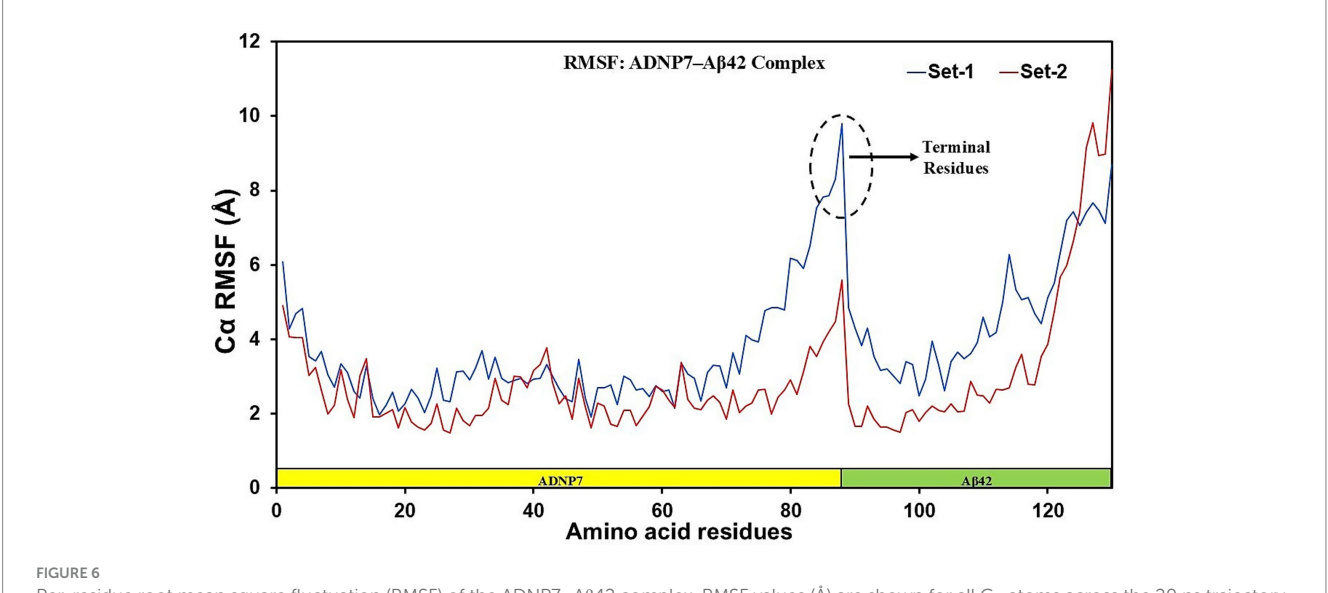
Complex	Simulation set	Energy components				
		$\Delta E_{vdw}$	$\Delta E_{ele}$	$\Delta G_{pol}$	$\Delta G_{non-pol}$	$\Delta G_{Total}$
ADNP7-Aβ42 Complex	Set-1	-91.202	-183.533	234.711	-10.592	-50.616
	Set-2	-90.955	-157.935	212.805	-10.485	-46.570



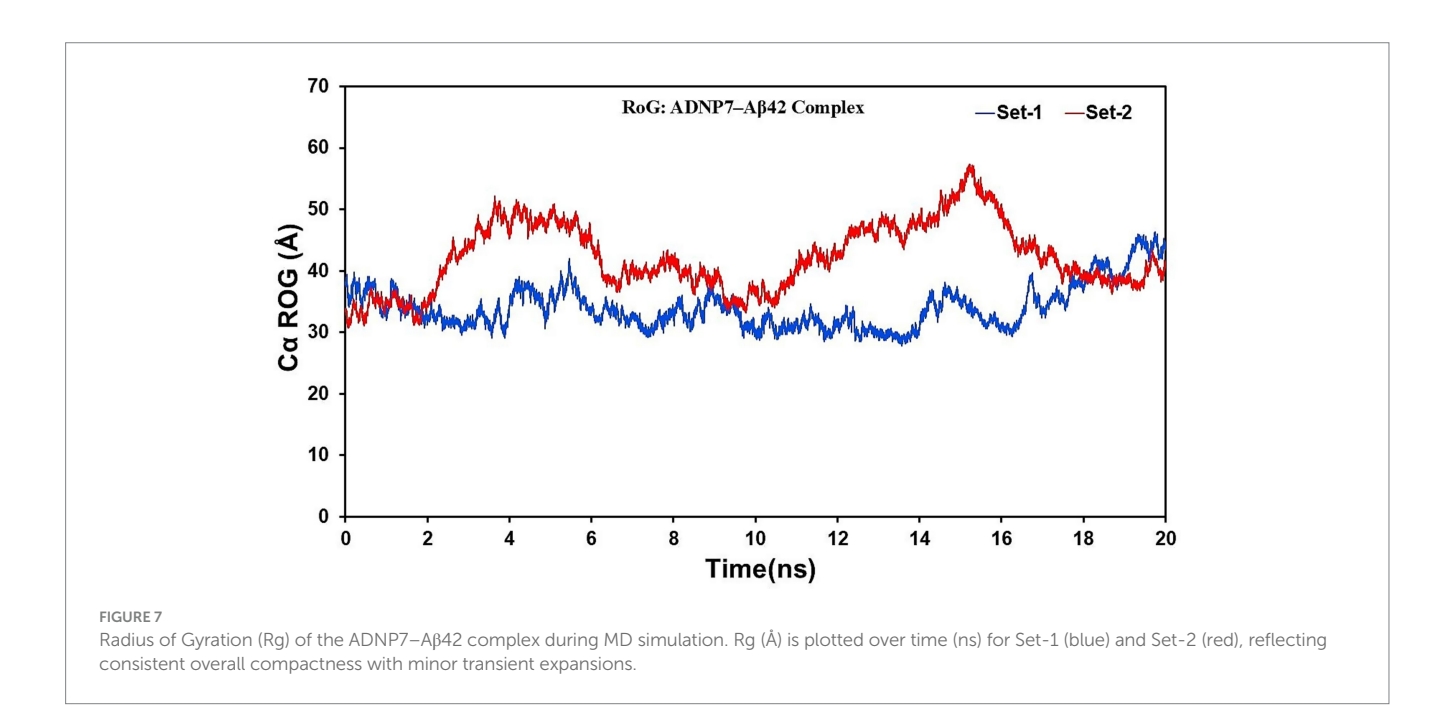
compact states after 18 ns, indicating convergence to equilibrated conformations. The Rg and RMSF analyses collectively indicate that ADNP7 forms a stable and compact complex with A $\beta$ 42, with dynamic variations predominantly occurring in the terminal and loop regions. The peptide is likely to stabilize at the central core of the complex while permitting conformational flexibility in surrounding residues.

## 3.5.4 Binding free energy analysis by MM/PBSA

Binding free energy calculations utilizing the MM/PBSA method were conducted on the final 20 ns of both MD simulations to assess the interaction intensity between ADNP7 and A $\beta$ 42. The total binding free energy ( $\Delta G_{Total}$ ) was determined to be significantly negative in both trials, -50.616 kcal/mol (Set1) and -46.570 kcal/mol (Set2) which are mentioned in the Table 4, signifying a stable and energetically



Per-residue root mean square fluctuation (RMSF) of the ADNP7-A $\beta$ 42 complex. RMSF values (Å) are shown for all C $\alpha$  atoms across the 20 ns trajectory for Set-1 (blue) and Set-2 (red). The ADNP7 segment (residues 1-88, yellow highlight) exhibits lower flexibility than the A $\beta$ 42 segment (residues 89-130, green highlight).

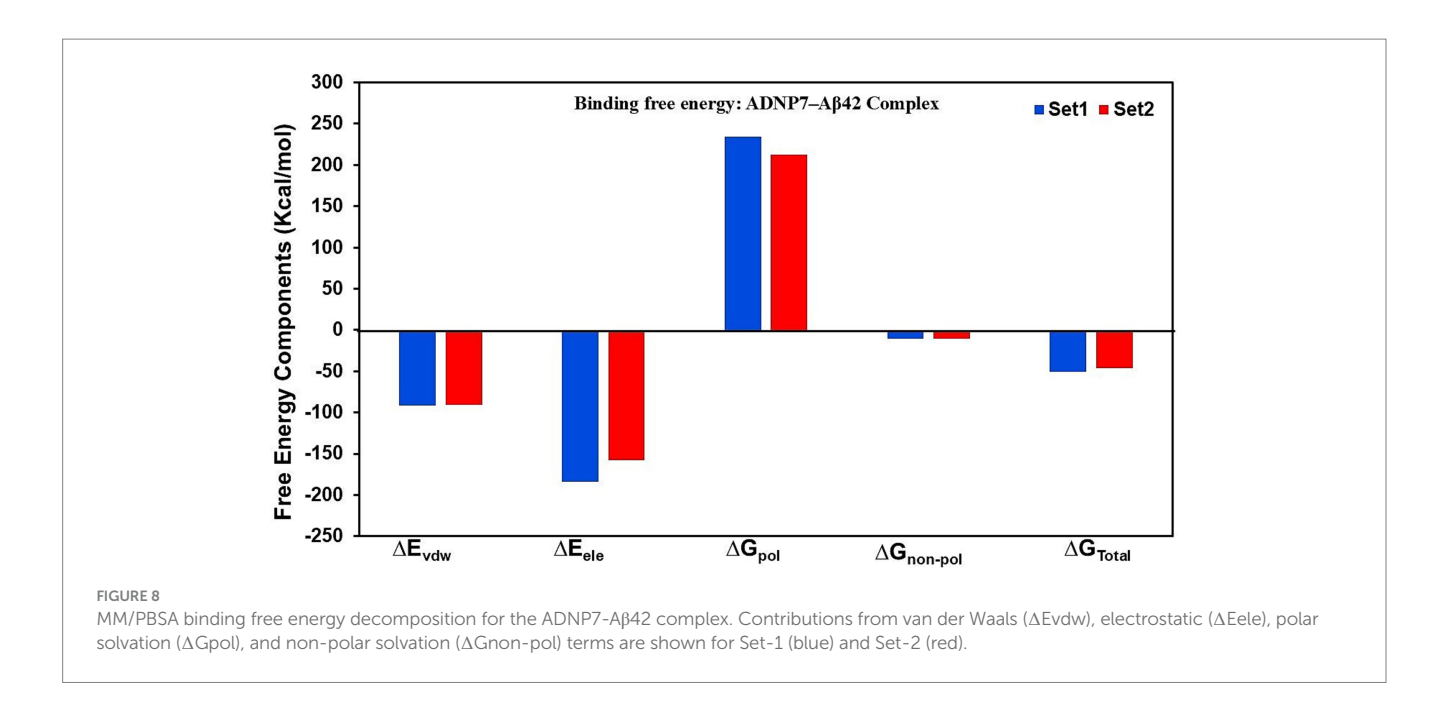


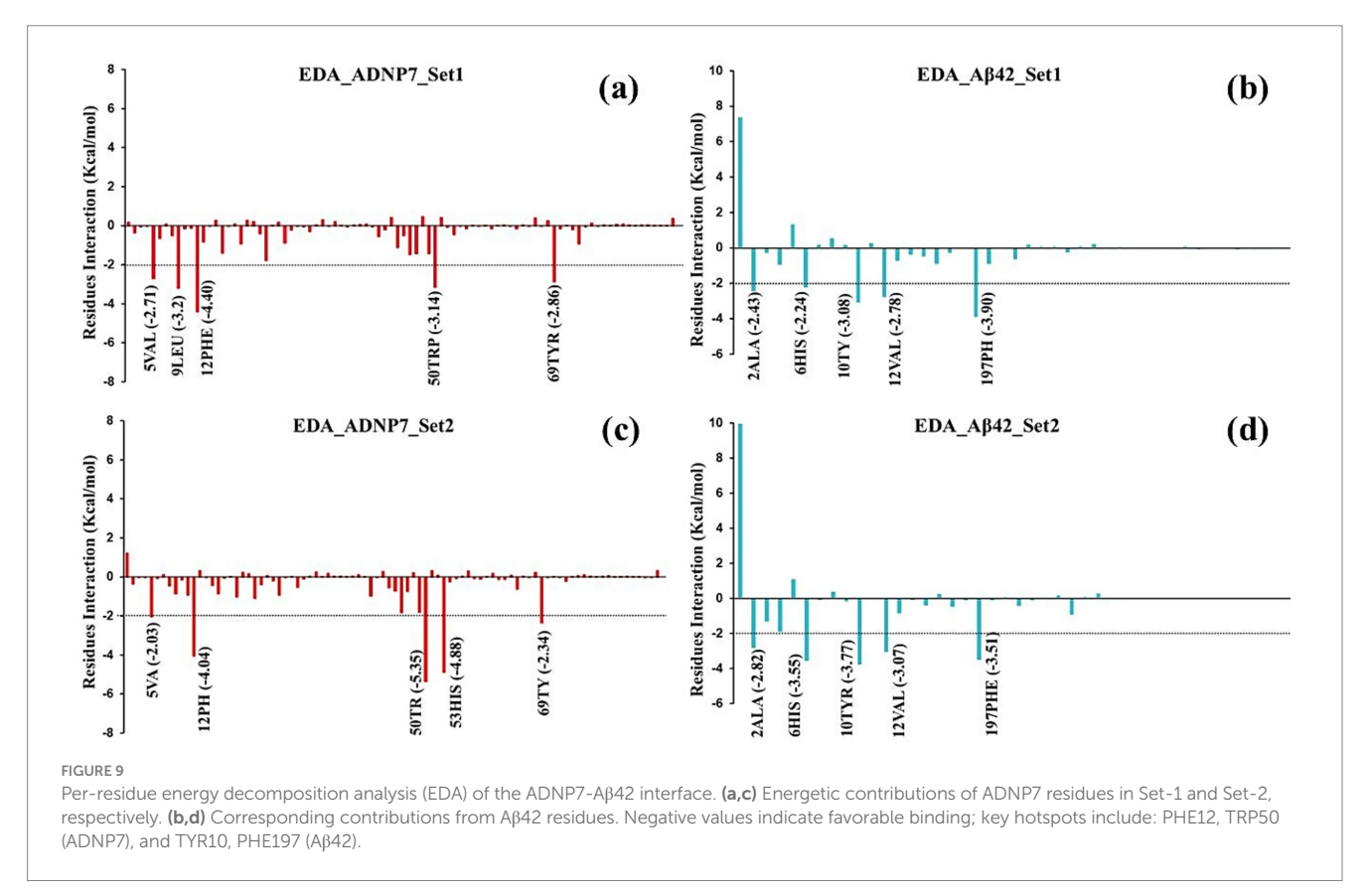
advantageous complex. The van der Waals  $(\Delta E_{vdw})$  and electrostatic  $(\Delta E_{ele})$  components were the primary contributors to binding, with values about -90 to -95 kcal/mol and -178 to -198 kcal/mol, respectively, underscoring robust hydrophobic packing and charge interactions. Conversely, the polar solvation energy  $(\Delta G_{pol})$  was detrimental (+211 to +225 kcal/mol), indicating the desolvation expense of polar residues. The non-polar solvation energy  $(\Delta G_{non-pol})$  offered negligible beneficial contributions, approximately in the range of -7 kcal/mol. The similarity across both sets suggests that ADNP7 consistently and robustly interacts with A $\beta$ 42, mostly because to hydrophobic and electrostatic interactions, notwithstanding solvation penalties (Figure 8).

# 3.5.5 Energy decomposition analysis (EDA)

Per-residue energy decomposition analysis (EDA), utilizing MM/ PBSA energy terms was conducted to identify the critical residues that contribute to the binding interface and stability of the ADNP7–A $\beta$ 42 complex. Figures 9a–d presents the outcomes of two independent MD simulation runs (Set1 and Set2), emphasizing the most energetically relevant residues from both ADNP7 (red bars) and A $\beta$ 42 (blue bars).

In Set1, the most advantageous binding residues in ADNP7 were PHE12 ( $-4.40~\rm kcal/mol$ ), LEU9 ( $-3.20~\rm kcal/mol$ ), TRP50 ( $-3.14~\rm kcal/mol$ ), TYR69 ( $-2.86~\rm kcal/mol$ ), and VAL5 ( $-2.71~\rm kcal/mol$ ) (Figure 9a). The residues are predominantly hydrophobic and aromatic, indicating that hydrophobic interactions and  $\pi$ -stacking play





a substantial role in ADNP7's attachment to  $A\beta$ 42. In the associated A $\beta$ 42 profile (Figure 9b), significant interacting residues included PHE197 (-3.90 kcal/mol), TYR10 (-3.08 kcal/mol), VAL12 (-2.78 kcal/mol), and ALA2 (-2.43 kcal/mol). The residues are primarily hydrophobic or aromatic, underscoring the preeminence of van der Waals interactions at the binding contact. In Set2, exploratory data analysis revealed a consistent interaction profile with certain variances in residue contributions. In ADNP7 (Figure 9c), the most prominent residues were TRP50 (-5.35 kcal/mol), HIS53 (-4.88 kcal/

mol), PHE12 (-4.04 kcal/mol), and VAL5 (-2.03 kcal/mol). These residues exhibited significant interaction energies in both sets, affirming their essential role in the stability of the complex. In relation to Aβ42 (Figure 9d), the residues exhibiting consistently robust binding included PHE197 (-3.51 kcal/mol), TYR10 (-3.77 kcal/mol), VAL12 (-3.07 kcal/mol), ALA2 (-2.82 kcal/mol), and HIS6 (-3.55 kcal/mol). These residues are probably engaged in hydrophobic interactions and  $\pi$ - $\pi$  stacking with the aromatic residues of ADNP7. The EDA data indicate that the binding surface is primarily stabilized

by hydrophobic and  $\pi$ -stacking interactions, with certain aromatic and aliphatic residues continuously yielding the highest negative interaction energy. The consistency of significant residue contributions across both simulation sets bolsters confidence in the reliability of the interaction model. The persistent engagement of PHE12 and TRP50 in ADNP7, alongside PHE197 and TYR10 in Aβ42, suggests that these residues may constitute essential binding hotspots, which might be targeted or altered in forthcoming peptide optimization research.

# 4 Discussion

Alzheimer's disease (AD) is characterized by amyloid- $\beta$  (A $\beta$ ) aggregation, which remains an important therapeutic challenge. Despite extensive research into small molecules, antibodies, and enzyme-based strategies, clinical efficacy has been limited. Here we present a two-stage BiLSTM generative framework that, when combined with physicochemical filtering, structural modeling, docking, and molecular dynamics (MD), and enables de novo peptide design. Applied to Aβ42, the framework generated 11 AI-Designed Novel Peptides (ADNPs), with ADNP7 showing the most favorable docking score, stable MD trajectories, and strong binding free energy supported by hydrophobic and aromatic interactions. Compared with earlier work using LSTM or CNN-BiLSTM models for peptide classification and motif rediscovery, our approach emphasizes unbiased sequence generation validated at structural and energetic levels (Xiao et al., 2021; Li et al., 2022). This distinguishes it from template-driven strategies such as KLVFF-based inhibitors and receptor-binding studies, and from prior docking-only pipelines that risk false positives (Chafekar et al., 2007). Although we did not apply any intrinsic interpretability methods to our BiLSTM model, the framework avoids black-box behavior through staged biophysical validation: initial filtering by physicochemical properties (GRAVY, instability, entropy) ensures functional plausibility across all candidates, while detailed per-residue MM/PBSA energy decomposition, applied to the top candidate ADNP7 links specific residues (PHE12, TRP50) to hydrophobic and  $\pi$ -stacking interactions with A $\beta$ 42. These interactions recapitulate established amyloid-binding motifs, demonstrating that the model's outputs are grounded in known biophysical principles rather than arbitrary sequence generation. The multi-metric evaluation employed here, combining docking with MD stability and MM/PBSA energy decomposition, provides stronger evidence of candidate robustness. The MM/PBSA binding free energy for the ADNP7 - Aβ42 complex was consistently favorable across two independent 20-ns MD replicates, with a mean  $\Delta G_{\text{total}} \approx -46 \text{ to } -50 \text{ kcal/mol}$  (Set-1: -50.6 kcal/mol; Set-2: -46.6 kcal/mol). These values fall within the range reported for other computationally validated Aß inhibitors (Patel et al., 2021; Patel et al., 2022a; Patel et al., 2022b; Mall et al., 2022), supporting strong predicted binding affinity. The interaction is driven primarily by hydrophobic and aromatic contributions from ADNP7 residues PHE12 and TRP50, consistent with known amyloid-binding motifs. However, MM/PBSA estimates are derived under idealized simulation conditions and do not account for physiological complexities such as membrane environments, macromolecular crowding, or the conformational heterogeneity of oligomeric/ fibrillar Aβ species. Therefore, while these energies support the promise of ADNP7 as a potential peptide inhibitor, experimental validation will be essential to confirm its true therapeutic effectiveness. The compact size and sequence diversity of ADNPs suggest potential advantages for central nervous system delivery, while ADNP7's binding profile indicates possible interference with aggregation interfaces. Beyond AD, the framework is adaptable to other protein misfolding disorders. While the monomeric Aβ42 structure (PDB: 1IYT) provides a suitable template for initial computational screening, it is important to note that  $A\beta$  primarily exerts its neurotoxic effects in oligomeric and fibrillar forms during AD progression. These aggregated states present distinct conformational landscapes and additional binding epitopes that could influence peptide recognition. Therefore, the results reported here represent an early-stage prediction of peptide-Aβ affinity. Future studies will extend this pipeline to physiologically relevant oligomeric and fibrillar  $\ensuremath{A\beta}$  assemblies. Additionally, the short MD timescale (20 ns), while provides reliable initial convergence of of RMSD, Rg, and binding energy profiles across two independent replicates supporting the the observed interactions (e.g., PHE12 and TRP50), may be insufficient to fully sample slow conformational rearrangements or achieve complete equilibration of intrinsically disordered regions in Aβ42. future studies employing longertimescale simulations (≥100 ns) or enhanced sampling methods will be valuable to confirm the durability of these interactions under extended dynamic conditions. Further limitations include, reliance on computational scores without experimental validation, Key pharmacological properties such as stability, immunogenicity, and blood-brain barrier permeability remain untested. Future work should focus on experimental validation of binding with binding assays (e.g., surface plasmon resonance or ELISA) and clearance potential with aggregation inhibition assays (e.g., Thioflavin T fluorescence) and cellular Aβ uptake studies. Aditionally, longer simulations for dynamic insight, and integration of reinforcement learning or transformer-based protein models to further enhance design capability. In summary, this study introduces a scalable AI-simulation pipeline for peptide discovery. While ADNP7 represents a promising computational lead, the broader value lies in demonstrating how interpretable AI model frameworks combined with biophysical validation can advance therapeutic peptide design.

# 5 Conclusion

This study introduces a two-stage BiLSTM framework for *de novo* peptide design, demonstrated through the generation of candidates targeting amyloid- $\beta$  (A $\beta$ ). By integrating sequence generation with physicochemical filtering, structural modeling, docking, and molecular dynamics simulations, we identified 11 candidate peptides, with ADNP7 showing the most stable and energetically favorable interaction with A $\beta$ 42. These results highlight the capacity of deep learning–guided design, combined with physics-based validation, to capture sequence–structure features critical for targeting amyloid aggregation. While clearance potential was inferred from the GO annotations of the training data, experimental validation is required to confirm biological activity of true clearance, BBB permeability as well as binding with the amyloid beta monomer and oligomers. Future work should focus on *in vitro* binding and aggregation assays, cellular and

animal models to assess clearance, and evaluation of pharmacological properties including stability and blood-brain barrier permeability. Overall, this framework provides both prioritized peptide leads and a broadly generalizable strategy for accelerating therapeutic discovery in Alzheimer's disease and other protein misfolding disorders.

# Data availability statement

The original contributions presented in the study are included in the article/Supplementary material, further inquiries can be directed to the corresponding author.

# **Author contributions**

VY: Conceptualization, Formal analysis, Investigation, Methodology, Writing – original draft, Writing – review & editing. OD: Conceptualization, Data curation, Formal analysis, Software, Writing – original draft, Writing – review & editing. JD: Investigation, Methodology, Software, Validation, Visualization, Writing – original draft, Writing – review & editing. AG: Investigation, Methodology, Software, Validation, Visualization, Writing – original draft, Writing – review & editing. BM: Resources, Supervision, Writing – original draft, Writing – review & editing. SB: Data curation, Formal analysis, Resources, Software, Validation, Writing – original draft, Writing – review & editing. NK: Resources, Software, Supervision, Writing – original draft, Writing – review & editing.

# **Funding**

The author(s) declare that no financial support was received for the research and/or publication of this article.

# Acknowledgments

The authors wish to thank Mr. Ch. Malla Reddy, founder chairman of Malla Reddy group of institutions, and Dr. Ch. Bhadra Reddy, chairman, Malla Reddy Institute of Medical Sciences, for supporting this study. The authors would also like to thank the patients who participated in the study for their time and effort.

## References

Ashburner, M., Ball, C. A., Blake, J. A., Botstein, D., Butler, H., Cherry, J. M., et al. (2000). Gene ontology: tool for the unification of biology. *Nat. Genet.* 25, 25–29. doi: 10.1038/75556

Basak, J. M., Verghese, P. B., Yoon, H., Kim, J., and Holtzman, D. M. (2012). Low-density lipoprotein receptor represents an apolipoprotein E-independent pathway of a $\beta$  uptake and degradation by astrocytes. *J. Biol. Chem.* 287, 13959–13971. doi: 10.1074/jbc.M111.288746

Bell, R. D., Deane, R., Chow, N., Long, X., Sagare, A., Singh, I., et al. (2009). SRF and myocardin regulate LRP-mediated amyloid- $\beta$  clearance in brain vascular cells. *Nat. Cell Biol.* 11, 143–153. doi: 10.1038/ncb1819

Berglund, M., Raiko, T., Honkala, M., Kärkkäinen, L., Vetek, A., and Karhunen, J. (2015). Bidirectional recurrent neural networks as generative models—reconstructing gaps in time series. Advances in Neural Information Processing Systems. 28, doi: 10.48550/arXiv.1504.01575

Berman, H. M., Westbrook, J., Feng, Z., Gilliland, G., Bhat, T. N., Weissig, H., et al. (2000). The Protein Data Bank. *Nucleic Acids Res.* 28, 235–242. doi: 10.1093/nar/28.1.235

Case, D. A., Ben-Shalom, I. Y., Brozell, S. R., Cerutti, D. S., Cheatham III, T. E., Cruzeiro, V. W. D., et al. (2018). Amber 2018. San Francisco: University of California. doi: 10.13140/RG.2.2.31525.68321

# Conflict of interest

The authors declare that the research was conducted in the absence of any commercial or financial relationships that could be construed as a potential conflict of interest.

The author(s) declared that they were an editorial board member of Frontiers, at the time of submission. This had no impact on the peer review process and the final decision.

# Generative AI statement

The authors declare that Gen AI was used in the creation of this manuscript. While no generative AI was used in the scientific or computational aspects of this study, including study design, data generation, analysis, or interpretation, language-editing assistance from ChatGPT (OpenAI) and Qwen AI was employed during the final stages of manuscript preparation solely to improve grammatical clarity, sentence structure, and readability. The authors retain full responsibility for all scientific content and conclusions.

Any alternative text (alt text) provided alongside figures in this article has been generated by Frontiers with the support of artificial intelligence and reasonable efforts have been made to ensure accuracy, including review by the authors wherever possible. If you identify any issues, please contact us.

# Publisher's note

All claims expressed in this article are solely those of the authors and do not necessarily represent those of their affiliated organizations, or those of the publisher, the editors and the reviewers. Any product that may be evaluated in this article, or claim that may be made by its manufacturer, is not guaranteed or endorsed by the publisher.

# Supplementary material

The Supplementary material for this article can be found online at: https://www.frontiersin.org/articles/10.3389/frai.2025.1709505/full#supplementary-material

Chafekar, S. M., Malda, H., Merkx, M., Meijer, E. W., Viertl, D., Lashuel, H. A., et al. (2007). Branched KLVFF tetramers strongly potentiate inhibition of  $\beta$ -amyloid aggregation. *Chembiochem* 8, 1857–1864. doi: 10.1002/cbic.200700338

Cho, H. S., Hyman, B. T., Greenberg, S. M., and Rebeck, G. W. (2001). Quantitation of apoE domains in Alzheimer disease brain suggests a role for apoE in a $\beta$  aggregation. *J. Neuropathol. Exp. Neurol.* 60, 342–349. doi: 10.1093/jnen/60.4.342

Choucair-Jaafar, N., Laporte, V., Levy, R., Poindron, P., Lombard, Y., and Gies, J.-P. (2011). Complement receptor 3 (CD11b/CD18) is implicated in the elimination of  $\beta$ -amyloid peptides: CR3 and  $\beta$ -amyloid peptides phagocytosis. *Fundam. Clin. Pharmacol.* 25, 115–122. doi: 10.1111/j.1472-8206.2010.00811.x

Citron, M. (2010). Alzheimer's disease: strategies for disease modification. *Nat. Rev. Drug Discov.* 9, 387–398. doi: 10.1038/nrd2896

Crescenzi, O., Tomaselli, S., Guerrini, R., Salvadori, S., D'Ursi, A. M., Temussi, P. A., et al. (2002). Solution structure of the Alzheimer amyloid  $\beta$ -peptide (1–42) in an apolar microenvironment: similarity with a virus fusion domain. *Eur. J. Biochem.* 269, 5642–5648. doi: 10.1046/j.1432-1033.2002.03271.x

- Fabrizio, C., Termine, A., Caltagirone, C., and Sancesario, G. (2021). Artificial intelligence for Alzheimer's disease: promise or challenge? *Diagnostics* 11:1473. doi: 10.3390/diagnostics11081473
- Fändrich, M., Meinhardt, J., and Grigorieff, N. (2009). Structural polymorphism of Alzheimer a $\beta$  and other amyloid fibrils. *Prion* 3, 89–93. doi: 10.4161/pri.3.2.8859
- Finder, V. H., and Glockshuber, R. (2007). Amyloid- $\beta$  aggregation. Neurodegener Dis 4, 13–27. doi: 10.1159/000100355
- França, V. L. B., Bezerra, E. M., da Costa, R. F., Carvalho, H. F., Freire, V. N., and Matos, G. (2024). Alzheimer's disease immunotherapy and mimetic peptide design for drug development: mutation screening, molecular dynamics, and a quantum biochemistry approach focusing on Aducanumab:: $a\beta_{2-7}$  binding affinity. ACS Chem. Neurosci. 15, 3543–3562. doi: 10.1021/acschemneuro.4c00453
- Funke, S. A., and Willbold, D. (2012). Peptides for therapy and diagnosis of Alzheimer's disease. *Curr. Pharm. Des.* 18, 755–767. doi: 10.2174/138161212799277752
- Goyal, D., Shuaib, S., Mann, S., and Goyal, B. (2017). Rationally designed peptides and peptidomimetics as inhibitors of amyloid- $\beta$  (a $\beta$ ) aggregation: potential therapeutics of Alzheimer's disease. *ACS Comb. Sci.* 19, 55–80. doi: 10.1021/acscombsci.6b00116
- Guruprasad, K., Reddy, B. V. B., and Pandit, M. W. (1990). Correlation between stability of a protein and its dipeptide composition: a novel approach for predicting in vivo stability of a protein from its primary sequence. *Protein Eng.* 4, 155–161. doi: 10.1093/protein/4.2.155
- Herráez, A. (2006). Biomolecules in the computer: Jmol to the rescue. *Biochem. Mol. Biol. Educ.* 34, 255–261. doi: 10.1002/bmb.2006.494034042644
- Hopkins, P. C. R., Sáinz-Fuertes, R., and Lovestone, S. (2011). The impact of a novel apolipoprotein E and amyloid- $\beta$  protein precursor-interacting protein on the production of amyloid- $\beta$ . J Alzheimer's Dis 26, 239–253. doi: 10.3233/JAD-2011-102115
- Husemann, J., Loike, J. D., Kodama, T., and Silverstein, S. C. (2001). Scavenger receptor class B type I (SR-BI) mediates adhesion of neonatal murine microglia to fibrillar β-amyloid. J. Neuroimmunol. 114, 142–150. doi: 10.1016/S0165-5728(01)00239-9
- Jeon, Y.-J., Won, H.-Y., Moon, M.-Y., Choi, W.-H., Chang, C.-H., Lee, J.-Y., et al. (2008). Interaction of microglia and amyloid-β through  $β_2$ -integrin is regulated by RhoA. *Neuroreport* 19, 1661–1665. doi: 10.1097/WNR.0b013e3283140f10
- Jiménez-García, B., Pons, C., and Fernández-Recio, J. (2013). pyDockWEB: a web server for rigid-body protein–protein docking using electrostatics and desolvation scoring. *Bioinformatics* 29, 1698–1699. doi: 10.1093/bioinformatics/btt262
- Jumper, J., Evans, R., Pritzel, A., Green, T., Figurnov, M., Ronneberger, O., et al. (2021). Highly accurate protein structure prediction with AlphaFold. *Nature* 596, 583–589. doi: 10.1038/s41586-021-03819-2
- Kanekiyo, T., Cirrito, J. R., Liu, C.-C., Shinohara, M., Li, J., Schuler, D. R., et al. (2013). Neuronal clearance of amyloid-β by endocytic receptor LRP1. *J. Neurosci.* 33, 19276–19283. doi: 10.1523/JNEUROSCI.3487-13.2013
- Kanekiyo, T., Liu, C.-C., Shinohara, M., Li, J., and Bu, G. (2012). LRP1 in brain vascular smooth muscle cells mediates local clearance of Alzheimer's amyloid-β. *J. Neurosci.* 32, 16458–16465. doi: 10.1523/JNEUROSCI.3987-12.2012
- Kaspar, A. A., and Reichert, J. M. (2013). Future directions for peptide therapeutics development. *Drug Discov. Today* 18, 807–817. doi: 10.1016/j.drudis.2013.05.011
- Kim, J., Castellano, J. M., Jiang, H., Basak, J. M., Parsadanian, M., Pham, V., et al. (2009). Overexpression of low-density lipoprotein receptor in the brain markedly inhibits amyloid deposition and increases extracellular a $\beta$  clearance. *Neuron* 64, 632–644. doi: 10.1016/j.neuron.2009.11.013
- Kuperstein, I., Broersen, K., Benilova, I., Rozenski, J., Jonckheere, W., Debulpaep, M., et al. (2010). Neurotoxicity of Alzheimer's disease aβ peptides is induced by small changes in the Aβ42 to Aβ40 ratio. *EMBO J.* 29, 3408–3420. doi:10.1038/emboj.2010.211
- Kyte, J., and Doolittle, R. F. (1982). A simple method for displaying the hydropathic character of a protein. *J. Mol. Biol.* 157, 105–132. doi: 10.1016/0022-2836(82)90515-0
- Levites, Y., Das, P., Price, R. W., Rochette, M. J., Kostura, L. A., McGowan, E. M., et al. (2006). Anti-A $\beta$ 42- and anti-A $\beta$ 40-specific mAbs attenuate amyloid deposition in an Alzheimer disease mouse model. *J. Clin. Invest.* 116, 193–201. doi: 10.1172/JCI25410
- Li, Y., Li, X., Liu, Y., Yao, Y., and Huang, G. (2022). MPMABP: a CNN and bi-LSTM-based method for predicting multi-activities of bioactive peptides. *Pharmaceuticals* 15:707. doi: 10.3390/ph15060707
- Llovera, R. E., de Tullio, M. B., Alonso, L. G., Leissring, M. A., Kaufman, S. B., Roher, A. E., et al. (2008). The catalytic domain of insulin-degrading enzyme forms a denaturant-resistant complex with amyloid  $\beta$  peptide: implications for Alzheimer disease pathogenesis. *J. Biol. Chem.* 283, 17039–17048. doi: 10.1074/jbc.M706316200
- Lowe, T. L., Strzelec, A., Kiessling, L. L., and Murphy, R. M. (2001). Structure-function relationships for inhibitors of  $\beta$ -amyloid toxicity containing the recognition sequence KLVFF. Biochemistry 40, 7882–7889. doi: 10.1021/bi002734u
- Mall, S., Srivastava, R., Sharma, N., Patel, C. N., Rolta, R., Sourirajan, A., et al. (2022). Antihypertensive activity of phytocompounds from selected medicinal plants via inhibition of angiotensin-converting enzyme (ACE) protein: an in-silico approach. *Nat. Prod. Res.* 36, 4526–4529. doi: 10.1080/14786419.2021.1990917
- Mandal, P. K., Pettegrew, J. W., Masliah, E., Hamilton, R. L., and Mandal, R. (2006). Interaction between a $\beta$  peptide and  $\alpha$  synuclein: molecular mechanisms in overlapping pathology of Alzheimer's and Parkinson's in dementia with Lewy body disease. *Neurochem. Res.* 31, 1153–1162. doi: 10.1007/s11064-006-9140-9

- Mayeux, R., Honig, L. S., Tang, M.-X., Manly, J., Stern, Y., Schupf, N., et al. (2003). Plasma A $\beta$ 40 and A $\beta$ 42 and Alzheimer's disease: relation to age, mortality, and risk. Neurology 61, 1185–1190. doi: 10.1212/01.WNL.0000091890.32140.8F
- McGregor, D. P. (2008). Discovering and improving novel peptide therapeutics. *Curr. Opin. Pharmacol.* 8, 616–619. doi: 10.1016/j.coph.2008.06.002
- McQuade, A., Kang, Y. J., Hasselmann, J., Coburn, M., Shabestari, S. K., Chadarevian, J. P., et al. (2020). Gene expression and functional deficits underlie TREM2-knockout microglia responses in human models of Alzheimer's disease. *Nat. Commun.* 11:5370. doi: 10.1038/s41467-020-19227-5
- Miners, J. S., Baig, S., Palmer, J., Palmer, L. E., Kehoe, P. G., and Love, S. (2008). Aβ-degrading enzymes in Alzheimer's disease. *Brain Pathol.* 18, 240–252. doi: 10.1111/j.1750-3639.2008.00132.x
- Morgan, D. (2011). Immunotherapy for Alzheimer's disease. J. Intern. Med. 269, 54-63. doi: 10.1111/j.1365-2796.2010.02315.x
- Narayan, P., Orte, A., Clarke, R. W., Bolognesi, B., Hook, S., Ganzinger, K. A., et al. (2012). The extracellular chaperone clusterin sequesters oligomeric forms of the amyloid- $\beta_{1^-40}$  peptide. *Nat. Struct. Mol. Biol.* 19, 79–83. doi: 10.1038/nsmb.2191
- Nie, Q., Du, X.-G., and Geng, M.-Y. (2011). Small molecule inhibitors of amyloid  $\beta$  peptide aggregation as a potential therapeutic strategy for Alzheimer's disease. *Acta Pharmacol. Sin.* 32, 545–551. doi: 10.1038/aps.2011.14
- Patel, C. N., Kumar, S. P., Pandya, H. A., and Rawal, R. M. (2021). Identification of potential inhibitors of coronavirus hemagglutinin-esterase using molecular docking, molecular dynamics simulation and binding free energy calculation. *Mol. Divers.* 25, 421–433. doi: 10.1007/s11030-020-10135-w
- Patel, C. N., Kumar, S. P., Pandya, H. A., and Rawal, R. M. (2022a). Computational exploration of natural inhibitors against SARS-CoV-2 main protease: insights from docking, dynamics, and binding free energy analysis. *J. Biomol. Struct. Dyn.* 40, 7744–7761. doi: 10.1016/j.compbiomed.2022.106318
- Patel, C. N., Kumar, S. P., Pandya, H. A., and Rawal, R. M. (2022b). In silico identification of potential inhibitors against SARS-CoV-2 papain-like protease through virtual screening, molecular docking, and molecular dynamics simulation. *Comput. Biol. Med.* 151:106318. doi: 10.1016/j.compbiomed.2022.106318
- Scheltens, P., De Strooper, B., Kivipelto, M., Holstege, H., Chételat, G., Teunissen, C. E., et al. (2021). Alzheimer's disease. *Lancet* 397, 1577–1590. doi: 10.1016/s0140-6736(20)32205-4
- Shannon, C. E. (1948). A mathematical theory of communication. *Bell Syst. Tech. J.* 27, 379–423. doi: 10.1002/j.1538-7305.1948.tb01338.x
- Shimizu, E., Kawahara, K., Kajizono, M., Sawada, M., and Nakayama, H. (2008). IL-4-induced selective clearance of oligomeric  $\beta$ -amyloid peptide(1–42) by rat primary type 2 microglia. *J. Immunol.* 181, 6503–6513. doi: 10.4049/jimmunol.181.9.6503
- Sievers, F., and Higgins, D. G. (2014). "Clustal omega, accurate alignment of very large numbers of sequences" in Multiple sequence alignment methods. ed. D. J. Russell (New York: Humana Press), 105–116.
- The UniProt Consortium (2021). UniProt: the universal protein knowledgebase in 2021. *Nucleic Acids Res.* 49, D480–D489. doi: 10.1093/nar/gkaa1100
- Tomaselli, S., Esposito, V., Vangone, P., van Nuland, N. A. J., Bonvin, A. M. J. J., Guerrini, R., et al. (2006). The  $\alpha$ -to- $\beta$  conformational transition of Alzheimer's a $\beta$ -(1–42) peptide in aqueous media is reversible: a step-by-step conformational analysis suggests the location of  $\beta$  conformation seeding. *Chembiochem* 7, 257–267. doi: 10.1002/cbic.200500223
- Urbanc, B., Cruz, L., Ding, F., Sammond, D., Khare, S., Buldyrev, S. V., et al. (2004). Molecular dynamics simulation of amyloid  $\beta$  dimer formation. *Biophys. J.* 87, 2310–2321. doi: 10.1529/biophysj.104.040980
- Vekrellis, K., Ye, Z., Qiu, W. Q., Walsh, D., Hartley, D., Chesneau, V., et al. (2000). Neurons regulate extracellular levels of amyloid  $\beta$ -protein via proteolysis by insulin-degrading enzyme. *J. Neurosci.* 20, 1657–1665. doi: 10.1523/JNEUROSCI.20-05-01657.2000
- Weggen, S., Rogers, M., and Eriksen, J. (2007). NSAIDs: small molecules for prevention of Alzheimer's disease or precursors for future drug development? *Trends Pharmacol. Sci.* 28, 536–543. doi: 10.1016/j.tips.2007.09.004
- Xiao, X., Shao, Y.-T., Cheng, X., and Stamatovic, B. (2021). iAMP-CA2L: a new CNN-BiLSTM-SVM classifier based on cellular automata image for identifying antimicrobial peptides and their functional types. *Brief. Bioinform*. 22:bbab209. doi: 10.1093/bib/bbab209
- Yeh, F. L., Wang, Y., Tom, I., Gonzalez, L. C., and Sheng, M. (2016). TREM2 binds to apolipoproteins, including APOE and CLU/APOJ, and thereby facilitates uptake of amyloid-beta by microglia. *Neuron* 91, 328–340. doi: 10.1016/j.neuron.2016.06.015
- Younkin, S. G. (1998). The role of A $\beta$ 42 in Alzheimer's disease. J. Physiol. 92, 289–292. doi: 10.1016/S0928-4257(98)80035-1
- Zhang, H., Wei, W., Zhao, M., Ma, L., Jiang, X., Pei, H., et al. (2021). Interaction between a $\beta$  and tau in the pathogenesis of Alzheimer's disease. *Int. J. Biol. Sci.* 17, 2181–2192. doi: 10.7150/ijbs.57078
- Zhao, Z., Sagare, A. P., Ma, Q., Halliday, M. R., Kong, P., Kisler, K., et al. (2015). Central role for PICALM in amyloid- $\beta$  blood-brain barrier transcytosis and clearance. *Nat. Neurosci.* 18, 978–987. doi: 10.1038/nn.4025
- Zhao, Y., Wu, X., Li, X., Jiang, L.-L., Gui, X., Liu, Y., et al. (2018). TREM2 is a receptor for  $\beta$ -amyloid that mediates microglial function. *Neuron* 97, 1023–1031.e7. doi: 10.1016/j.neuron.2018.01.031